Composites Part B 248 (2023) 110377

Contents lists available at ScienceDirect

Composites Part B

journal homepage: www.elsevier.com/locate/compositesb

Flame-retardant and thermal-protective polyimide-hydroxyapatite aerogel fiber-based composite textile for firefighting clothing

Qiaoran Zhang [a], Lei Ma [a], Tiantian Xue [a], Jing Tian [a], Wei Fan [a,*], Tianxi Liu [a,b,**]

[a] State Key Laboratory for Modification of Chemical Fibers and Polymer Materials, College of Materials Science and Engineering, Donghua University, Shanghai, 201620, China

[b] Key Laboratory of Synthetic and Biological Colloids, Ministry of Education, School of Chemical and Material Engineering, Jiangnan University, Wuxi, 214122, China

ARTICLE INFO

Keywords:
Aerogel fiber
Polyimide
Phase change materials
Flame retardant
Thermal-protective

ABSTRACT

Firefighting protective clothing is an essential equipment for firefighters that can provide protection from all kinds of thermal hazards and prevent burn injuries. However, it is still a challenge to develop lightweight firefighting clothing without compromising their excellent fire-resistant and thermal-protective performance. In this study, we report a novel polyimide aerogel fiber-based double-layer smart textile comprising of flame-retardant outer layer (ambient-side) with excellent fire resistance and phase-changeable inner layer (next to skin side) with thermal-regulating function, achieving comprehensive flame-retardant and thermal-protective function. The polyimide-hydroxyapatite-reduced graphene oxide (PI-HAP-rGO) aerogel fabric (outer layer) acquires 54.7% and 70.0% reduction of peak heat release rate compared with that of pure PI aerogel fabric and commercial aramid fabric, respectively, exhibiting excellent fire resistance. The phase-changeable polyimide-hydroxyapatite/eicosane (PI-HAP/C20) fabric (inner layer) with high melting enthalpy of 193.2 J g^{-1} can delay the temperature rise by thermal buffering effects during the phase change process, endowing cool somatosensory temperature for firefighters. Consequently, the double-layer smart textile can extend the time (280.0 s) to pain threshold of human skin, much longer than that of the commercial aramid fabric (101.0 s) and glass fiber fabric (56.5 s), which exhibits huge potential for next-generation firefighting clothing.

1. Introduction

It is well known that firefighting protective clothing with excellent flame-retardant and thermal protective performance is critical to various activities, especially in the fire environment. Normally, the conventional firefighting protective garment contains multi-layer structure, assuring that firefighters are safe from the threats such as external heat flux as well as flame [1–3]. Unfortunately, the multi-layer design of the firefighting protective garment has a high self-weight and increases the difficulty of movement. Hence, it is urgent to develop a novel lightweight fabric with durable flame-retardant as well as thermal protective function, which is able to minimize the thermal stress and provide better safety for firefighters in hot and humid environment [4].

Aerogels, a good candidate for thermal protective materials, which are comprised of a porous solid and dispersed gaseous phase, have been studied by a boom of research, due to the advantages of high porosity, low thermal conductivity and lightweight [5–7]. Silica aerogels have been studied frequently as coatings for fire protective garment, due to their ultra-low thermal conductivity and non-flammable property. For instance, Qi et al. [8] has designed a silica aerogel embedded firefighting protective clothing with excellent thermal protective performance. Shaid et al. [9,10] has added SiO_2 aerogel nanoparticles to 65/35 wool/aramid blended fabric to improve its thermal protection performance, which reveals that only 2 wt% aerogel nanoparticles can increase the thermal resistance of the fabric by 68.7%. Although silica aerogels could enhance the thermal protection of fabric to some extent, they still face the common problems such as falling off of silica powder and poor mechanical strength. In recent studies, polyimide (PI) aerogel fiber-based fabric has received more and more attention, due to its unique characterizations such as excellent thermal stability, high mechanical strength and high porosity [11,12]. Particularly, its porous structure can endow the fabric with excellent thermal insulation and

* Corresponding author.
** Corresponding author. State Key Laboratory for Modification of Chemical Fibers and Polymer Materials, College of Materials Science and Engineering, Donghua University, Shanghai, 201620, China.
E-mail addresses: weifan@dhu.edu.cn (W. Fan), txliu@dhu.edu.cn, txliu@fudan.edu.cn (T. Liu).

https://doi.org/10.1016/j.compositesb.2022.110377
Received 5 August 2022; Received in revised form 9 October 2022; Accepted 22 October 2022
Available online 27 October 2022

ideal air permeability, showing its huge potential as firefighting protective fabric [13]. Recently, flame-retardant PI fabrics have been reported by introducing unique chemical structure via co-polymerization or surface treating by flame-retardant agents such as phosphoric acid [14,15]. Although PI fabrics exhibit superior flame-retardant effect than most polymer fabrics, the applications of organic PI fabrics are still limited by their poor fire resistance. To minimize the fire hazards of polymer, different kinds of inorganic flame retardants including graphene oxide [16,17], multi-walled carbon nanotubes [18], montmorillonite [19] and hydroxyapatite [20], have been compounded with polymer matrix. For example, Peng et al. [21] has synthesized novel sandwich-like cobalt borate nanosheets-molybdenum disulfide (CoBi–MoS_2) hybrids for improving the flame retardancy of polyacrylonitrile (PAN) composite fiber. Compared with pure PAN fiber, the peak heat release rate and peak smoke production rate of 2 wt% CoBi–MoS_2/PAN composite fiber are decreased by 46.2% and 45.7%, respectively. Wang et al. [22] has designed biomimetic structural composite aerogel by incorporating the hierarchical graphene-confined zirconium phosphate (ZrP/RGO) nanosheets, which exhibits high limited oxygen index (33.5%) and low peak heat release rate (14.1 kW m^{-2}). Therefore, it is of great importance to composite inorganic nanoparticles with PI aerogel fibers to enhance the flame-retardancy of PI aerogel fiber-based fabrics.

It is generally acknowledged that the pain threshold of human skin is around 44 °C, and severe burns will occur if the skin temperature is higher than the threshold temperature [10]. Therefore, to postpone the outside heat flux spreading to human skin is essential for firefighting clothing to further enhance the thermal protection. Phase change materials (PCMs), as active heat storage−release materials, can absorb/release energy in the form of latent heat through the phase change process, which exhibit huge potential in reducing the heat stress and prolonging fire rescue time, demonstrating great potential as temperature regulating materials for firefighting protective clothing [23–29]. Especially, organic PCMs have phase change temperature at around 18–65 °C that close to human body temperature with good recycling stability, making them more suitable for firefighting protective clothing. With the aim of preventing the leakage issue of PCMs during the phase change process, encapsulation of PCMs in the form of microcapsules has been proved a common and effective strategy. For example, Li et al. [30] has synthesized multifunctional microencapsulated PCM for intelligent textiles, and the resultant textile showed phase-change enthalpy of 36.8 J g^{-1}. Li et al. [31] has obtained flexible and photothermal polyurethane film by utilizing polydopamine-coated phase change microcapsules with relatively high enthalpy of 110 J g^{-1}. However, the microencapsulated PCM-coated garment has low loading of PCM, leading to limited energy storage and thermoregulation capability. Hence, it remains a huge challenge to effectively encapsulate the PCMs into the textile with high loading and endow the textile high enthalpy for effective thermoregulation.

In this work, a novel double-layer textile comprising of polyimide-hydroxyapatite-reduced graphene oxide (PI-HAP-rGO) aerogel fabric and polyimide-hydroxyapatite/eicosane (PI-HAP/C20) fabric has been designed with outstanding fire-resistance and thermal-protective performance for potential firefighting clothing. The PI-HAP-rGO aerogel fabric as outer layer exhibits excellent fire-resistant property that enhances the fire safety of firefighters, by incorporating the flame retardant materials of HAP and rGO into PI aerogel fabric. The PI-HAP/C20 as inner layer is designed by incorporating PCM into the porous structure of PI-HAP aerogel fiber, which shows strong thermoregulation capability. The highly porous structure of PI-HAP aerogel fiber endows high loading of C20, leading to high melting enthalpy, while the capillary force of PI-HAP aerogel fiber could prevent the leakage of C20 during the phase change process. Consequently, the resultant double-layer smart textile could delay the time to pain threshold significantly, compared with the commercial aramid fabric and glass fiber fabric, which could reduce the burning likelihood of firefighters, presenting great potential as exceptional candidates for firefighting protective clothing.

2. Experimental methods

2.1. Preparation of PI-HAP aerogel fiber

In a typical experiment, HAP nanoparticles were synthesized as follows [20]. A certain volume of ammonia was added into 0.1 mol L^{-1} Ca$(NO_3)_2$ $4H_2O$ aqueous solution, adjusting its pH to around 11. 0.1 mol L^{-1} $(NH_4)_2HPO_4$ aqueous solution was mixed with the above solution under a magnetic stirring, and make sure pH of the mixture maintaining 11 by the incorporation of ammonia. The reaction was completed after being stirred for 24 h, and then the HAP powder was obtained by filtering and washing with deionized water for several times.

According to our previous work [32], a water-soluble polyamic acid (PAA) with a solid content of 15 wt% was synthesized from 4,4′-oxydianiline and 3,3′,4,4′-biphenyl tetracarboxylic dianhydride with addition of triethylamine (TEA). PAA aqueous solution containing HAP nanoparticles with different concentration was mixed to obtain a uniform PAA-HAP spinning solution. Specifically, 1 g of PAA solid was added into the aqueous dispersion of HAP nanoparticles (5, 10, 15 and 20 mg mL^{-1}, respectively), and then 0.5 g of TEA as a cosolvent was incorporated with stirring, obtaining stable PAA-HAP spinning solution. PAA-HAP aerogel fiber was obtained via subsequent freeze-spinning technique according to our previous work [33]. The as-prepared PAA--HAP aerogel fiber was transferred into a tube furnace for thermal imidization at 100 °C, 200 °C and 300 °C respectively for 1 h in N_2 atmosphere, to obtain PI-HAP aerogel fibers. PI-HAP aerogel fibers with different content of HAP nanoparticles were denoted as PI-HAP_5, PI-HAP_{10}, PI-HAP_{15}, PI-HAP_{20}, respectively.

2.2. Preparation of PI-HAP-rGO aerogel fabric

Graphene oxide (GO) was obtained via typical Hummers' method according to previous work [34]. For further improving the fire resistance, the PI-HAP aerogel fiber was immersed into GO solution (5 mg mL^{-1}) for 10 min repeatedly with 2, 4, and 6 times, respectively, obtaining PI-HAP-GO-2, PI-HAP-GO-4, and PI-HAP-GO-6 aerogel fibers. Finally, PI-HAP-rGO aerogel fibers were prepared by thermal reduction at 250 °C for 2 h under N_2 atmosphere. And the resultant PI-HAP-rGO aerogel fabric was obtained by weaving PI-HAP-rGO aerogel fibers.

2.3. Preparation of phase-changeable PI-HAP/C20 fabric

Eicosane (C20) was heated at 80 °C until melting in a vacuum oven, and then PI-HAP aerogel fabric was immersed into the melting C20 for 6 h, with the aim of saturated adsorption of C20. Afterwards, the excess C20 attached to the surface of PI-HAP aerogel fabric was removed by transferring the sample onto the filter paper, obtaining phase-changeable PI-HAP/C20 fabric. The resultant smart textile with excellent firefighting and thermal-protective performance was fabricated by integrating two layers of PI-HAP-rGO aerogel fabric and phase-changeable PI-HAP/C20 fabric.

2.4. Characterizations

X-ray diffraction (XRD) patterns were detected by a 18 KW Turn Target X-ray Diffractometer (D2 PHASER, Germany) (Cu Kα radiation, λ = 0.15418 nm; voltage: 40 kV, current: 40 mA). Fourier transform infrared spectra (FT-IR) was recorded with a Nicolet6700 FT-IR spectrophotometer (Bruker Spectrum Instruments, USA) in the wavenumber range of 550–4000 cm^{-1}. The morphology as well as the relative EDS mapping image of PI and its composite fabric was observed by field-emission scanning electron microscopy (SEM, FESEM-7500F, Japan). A transmission electron microscope (TEM, JEM-2100, Japan) was

performed to observe the microstructure of HAP nanoparticles. The thermogravimetric analysis (TGA) of the as-prepared samples was conducted by thermogravimetric analyzer (Netzsch TG 209 F1 Libra, Germany) under nitrogen atmosphere. Differential scanning calorimetry (Q20 DSC, USA) was utilized for characterizing the phase changeable behaviors of C20, PI-HAP/C20 samples. And the corresponding enthalpy values were calculated from the DSC plots.Tensile tests were carried out on an electronic universal testing instrument (UTM2102, China).

Micro-cone calorimetry (MCC-2, Govmark, USA) was utilized to test the fire resistance of PI and its composite aerogel fabrics as well as commercial aramid fabric. The limited oxygen index (LOI) was evaluated by using an oxygen index meter (JF-3, China) according to ASTM Standard D2863. Raman spectra was conducted to analyze the graphitic degree of the residual char after burning tests by utilizing inVia-Reflex Raman spectrometer (Renishaw Company, UK). The thermal insulation performance was evaluated by thermocouple (175T2, testo Co., Ltd, China) and thermal imaging camera (FOTRIC 226s, China), for detecting the temperature distribution of the textiles.

3. Results and discussions

Fig. 1a shows the typical experimental procedure for preparing firefighting and thermal-protective textile containing the outer layer of PI-HAP-rGO aerogel fabric and inner layer of phase-changeable PI-HAP/C20 fabric. Specifically, PI-HAP aerogel fiber with a highly porous structure was obtained via freeze-spinning and thermal imidization from PAA-HAP spinning solution. And the PI-HAP-rGO aerogel fabric was prepared by coating of rGO layer and subsequent weaving, which serves as the firefighting outer layer of the smart textile. Besides, the PI-HAP aerogel fiber with the highly porous structure can allow to encapsulate C20, obtaining phase-changeable PI-HAP/C20 fabric which serves as the thermal-regulative inner layer. As illustrated in Fig. 1b, smart textile with excellent firefighting and thermal-protective performance is composed of double layers with two main criteria: (i) the outer layer with fire resistance properties could enhance the fire safety for firefighters; (ii) the inner layer containing PCM could postpone the temperature change to ensure the thermal protective performance of firefighters in hot environment. As displayed in Fig. 1c, the outer layer of PI-HAP-rGO aerogel fabric exhibits good flexibility and fire resistance, providing the possibility as wearable clothing. Moreover, the resultant double-layer textile can effectively block the fire spreading and inhibit heat transfer (Fig. 1d). With the smart textile as a protection, a flower can stand well on its surface without damage after ignition for 60 s on the alcohol lamp, indicating its excellent fire-resistant and thermal-protective properties, providing great safety for wearers at fire scene.

3.1. Flame-retardant performance of PI-HAP-rGO aerogel fabric

As for the flame-retardant outer layer of the smart textile, the high-temperature resistance and flame-retardant performance are desired (Fig. 2a). Lightweight and mechanically strong PI-HAP-rGO aerogel fiber with highly porous structure is designed, in which HAP nanoparticles can improve the thermal stability and rGO layer can enhance the fire resistance. The morphology of PI, PI-HAP and PI-HAP-rGO aerogel fibers were observed by SEM images given in Fig. 2b. As shown in Fig. 2b, PI, PI-HAP and PI-HAP-rGO aerogel fibers present highly porous structure, which is formed by the sublimation of ice crystal during freeze-spinning and freeze-drying. The addition of HAP does not have obvious influence on the morphology of the aerogel fiber due to the small size of HAP nanoparticles (50 nm, Fig. S1). Nevertheless, the typical P and Ca elements in HAP are detected by corresponding EDS images (Fig. S2), which are dispersed uniformly in the porous structure of PI-HAP, demonstrating the good dispersion of HAP nanoparticles among the composite aerogel fiber. As for PI-HAP-rGO aerogel fiber, a uniform thin layer with thickness about 2 μm is well coated on the surface of PI-HAP aerogel fiber, demonstrating the successful coating of multilayered rGO sheets on the aerogel fiber. Moreover, PI-HAP aerogel fibers exhibit enhanced tensile strength, compared with that

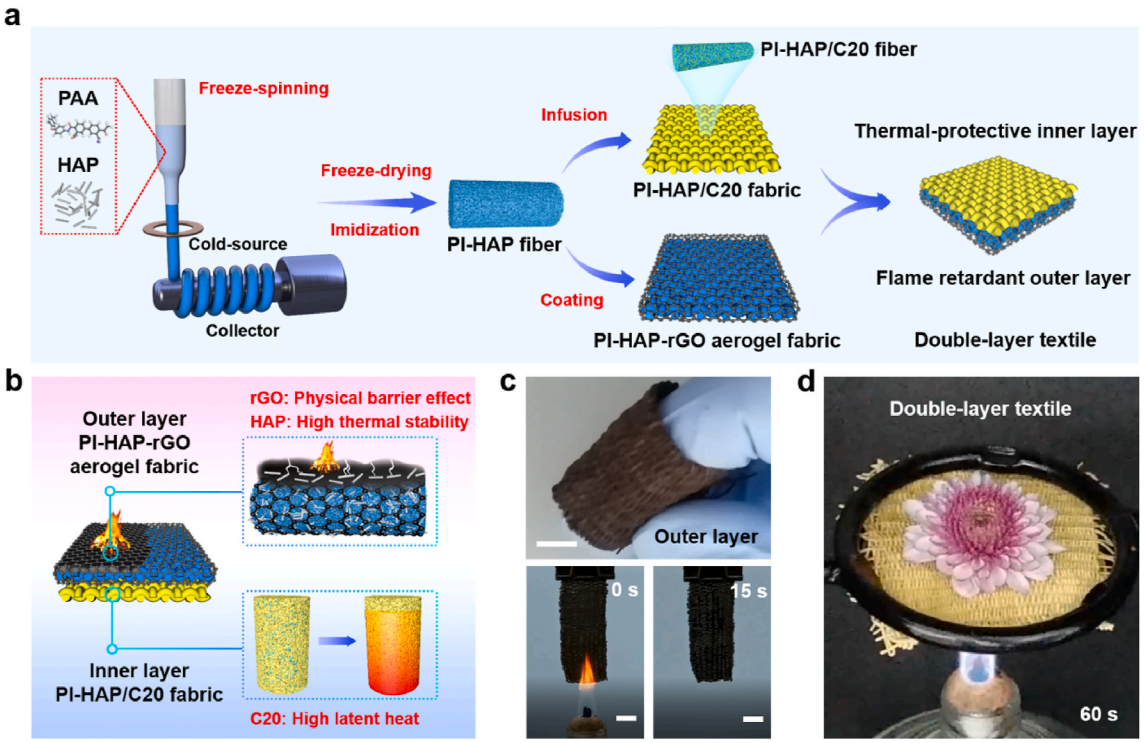

Fig. 1. (a) Schematic illustration of fabrication of double-layer textile comprising of PI-HAP-rGO aerogel fabric and PI-HAP/C20 fabric. (b) Schematic illustration of the function of double-layer textile. (c) Photographs of PI-HAP-rGO aerogel fabric before and after ignition for 15 s, reflecting its good flexibility and fire resistance (scale bar = 10 mm). (d) Photographs of the double-layer textile supporting a flower on alcohol lamp, reflecting its excellent thermal-protective performance.

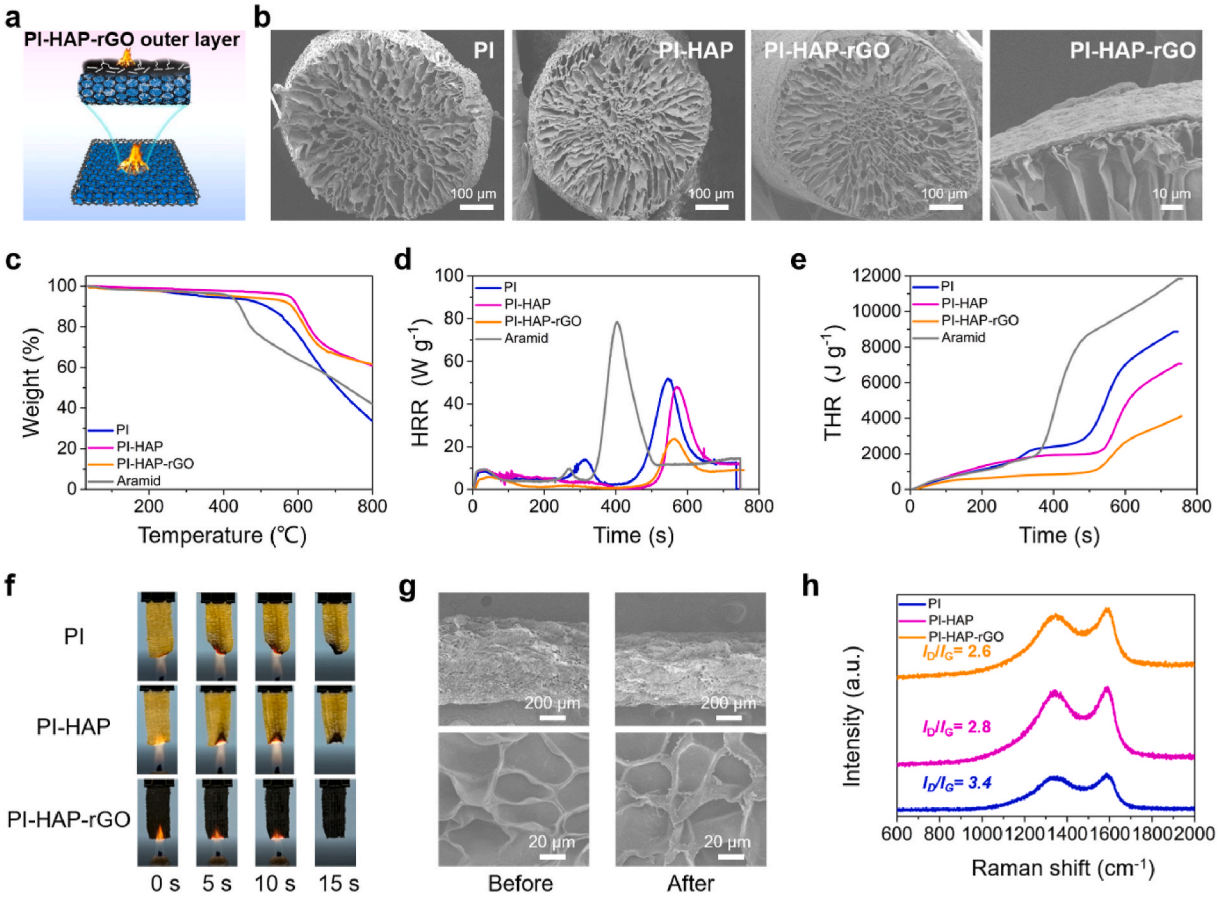

Fig. 2. Flame-retardant performance of PI-HAP-rGO aerogel fabric outer layer. (a) Schematic illustration of PI-HAP-rGO aerogel fabric with flame retardancy. (b) Radial cross-sectional SEM images of PI, PI-HAP and PI-HAP-rGO aerogel fibers. (c) TG curves, (d) HRR curves and (e) THR curves of aerogel fibers and commercial aramid fibers. (f) Optical images of aerogel fabrics during the vertical burning tests. (g) SEM images of PI-HAP-rGO aerogel fibers before and after combustion. (h) Raman spectra of char residues of PI, PI-HAP and PI-HAP-rGO aerogel fabrics.

of pure PI aerogel fiber as shown in Fig. S3. PI-HAP$_{15}$ aerogel fiber presents optimized tensile strength of up to 29.1 ± 0.8 MPa, which is selected for further research. Besides, PI-HAP-rGO aerogel fiber still maintains high strength of 19.2 ± 0.5 MPa, and much improved break elongation, mainly due to the good physical interaction between rGO coating and PI aerogel fiber, which is beneficial for further weaving.

Thermal stability and thermal decomposition behavior of PI and its composite fibers were given in Fig. 2c, and the relevant data was summarized in Table S1. It is noted that PI-HAP aerogel fiber has much higher $T_{-5\%}$ (575.7 °C) and T_{max} (612.8 °C) than that of PI aerogel fiber (343.3 °C, 562.0 °C), indicating that HAP nanoparticles can largely improve the thermal stability of PI aerogel fiber. Besides, the residue of PI-HAP aerogel fibers is increased from 33.6 wt% to 60.9 wt% compared to that of pure PI aerogel fibers, reflecting strong contribution from HAP nanoparticles to the formation of thermally stable structure [35]. PI-HAP-rGO aerogel fiber presents a similar thermal stability, which has the excessive char residue up to 61.6 wt%. In addition, the decomposition temperature and char residue of PI-HAP-rGO aerogel fiber is much higher than that of commercial aramid fiber, commonly used for fire-protection clothing, indicating its excellent thermal stability for potential firefighting textile.

Flame-retardant performance and combustion behavior of the as-prepared aerogel fabrics were evaluated by LOI measurement and micro-cone calorimetry. As shown in Fig. S4, the LOI values of PI and its composite aerogel fibers were all above 27.0%, corresponding to non-flammable ability under air atmosphere [36]. The LOI value of PI-HAP is 39.8%, slightly increased as compared with PI, suggesting the introduction of HAP nanoparticles could enhance the fire resistance to some extent. For further enhancing the fire resistance, additional rGO layers are coated on PI-HAP aerogel fiber with LOI values further increased. With optimized layers of rGO, LOI value of PI-HAP-rGO-4 aerogel fiber is as high as 47.5%, which is much higher than that of commercial aramid fabric (30.6%) and polyimide fabric (34.8%) (Fig. S5), corresponding to outstanding flame-retardant effect. Furthermore, the PI-HAP-rGO aerogel fabric still has high LOI value of 47.0% after washing for 10 times, demonstrating durable flame retardancy (Table S2). The heat release rate (HRR) and total heat release (THR) curves of PI, PI-HAP and PI-HAP-rGO aerogel textile and commercial aramid fiber were depicted in Fig. 2d and **e**, respectively, and the related combustion parameters such as peak heat release rate (PHRR), THR and time to PHRR were given in Table S3. PI aerogel fabric released heat slowly after ignition with a peak heat release rate (PHRR) value of 52.1 W g^{-1} as well as a THR value of 9.1 kJ g^{-1}. After incorporating of HAP nanoparticles and coating rGO layers, much decreased PHRR value (23.8 W g^{-1}) as well as the THR value (4.9 kJ g^{-1}) can be observed for PI-HAP-rGO aerogel fabric, corresponding to a vigorous reduction of 54.3% and 46.1% respectively in comparison to that of PI aerogel fabric, manifesting the huge suppression of heat spreading when burning. In addition, compared with that of commercial aramid fabric, there exist 70.0% reduction of PHRR, 58.8% reduction of THR and much longer time to PHRR for PI-HAP-rGO aerogel fabric, respectively, exhibiting outstanding fire safety. Moreover, the flame-retardant performance of our aerogel fabrics can be intuitively observed from vertical combustion test as exhibited in Fig. 2f and **Videos S1–S3**. As observed in Fig. 2f, PI and PI-HAP aerogel fabrics were easier to ignite, and slight shrinkage was observed after burning for 10 s. In contrast, PI-HAP-rGO aerogel

fabric could not be ignited after burning by an alcohol lamp, and maintained the original shape and size without obvious combustion and shrinkage, presenting superior fire resistance compared to that of commercial aramid, polyimide and glass fiber fabric. It could be observed that the PI-HAP-rGO aerogel fabric has no obvious change, while other commercial fabrics have occurred fierce burning with significant deforming (Fig. S6). This unique fire-resistant performance can be attributed to the synergistic effect of HAP nanoparticles with excellent thermal stability and rGO coating layer with physical barrier effect. Specifically, the HAP nanoparticles can improve the high-temperature resistance of PI aerogel fabric, due to its superior thermal stability and non-flammable performance. The rGO coating layer can serve as the physical barrier to block the oxygen diffusion into the PI-HAP aerogel fiber and prevent the escape of volatile products, thus suppressing the combustion of the aerogel fabric.

Supplementary video related to this article can be found at https://doi.org/10.1016/j.compositesb.2022.110377

The structure and morphology of PI, PI-HAP, and PI-HAP-rGO aerogel fabrics after combustion test were further evaluated. As shown in Fig. 2g, the morphology of PI-HAP-rGO aerogel fiber has no obvious change before and after ignition, indicating an ideal fire resistance. The graphitized degree of residue char was measured by Raman spectra, which was depicted in Fig. 2h. It is noted that all the samples present two broad peaks with maximum intensity at around 1365 and 1600 cm^{-1}, which are assigned to D (disordered carbons) and G (graphite crystalline) band, respectively. It is noted that PI-HAP-rGO aerogel fabric has the lowest I_D/I_G value of 2.6, comparing to 3.4 of PI and 2.8 of PI-HAP, indicating a high graphitization degree of char residue, which is mainly due to the increased content of graphite carbon with incorporation of rGO [37]. The high graphitic degree char covered on the surface could block or delay the transmission of heat flux and oxygen, and then prevent the underlying polymer from burning. Moreover, the presence of HAP could enhance the thermal oxidative resistance of the char residue [38]. Therefore, the PI-HAP-rGO aerogel fabric with excellent thermal stability and fire resistance can be potentially used as flame-retardant outer layer of firefighting clothing.

3.2. Thermoregulation performance of PI-HAP/C20 fabric

For improving the thermal protection performance, the inner layer of the double-layer textile is designed by incorporating PCM into the porous structure of PI-HAP aerogel fiber, which can regulate the temperature by storing or releasing heat (Fig. 3a). The cross-sectional SEM images of PI-HAP/C20 fiber (Fig. 3b) shows that the porous structure of PI-HAP aerogel fiber is filled by C20 significantly, leaving almost no pores exposed. As shown by FT-IR spectra (Fig. 3c), in addition to the

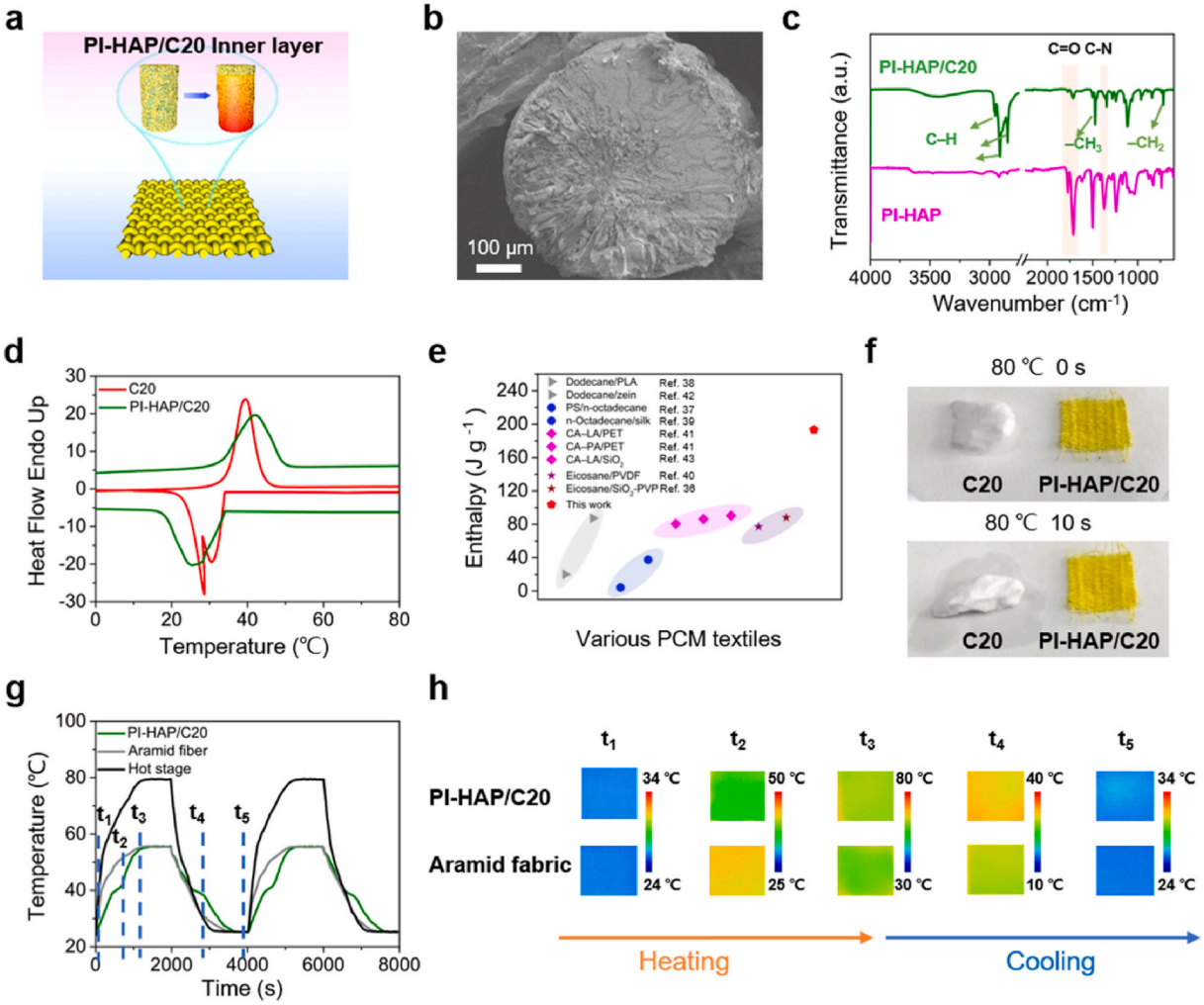

Fig. 3. Thermoregulation performance of PI-HAP/C20 fabric inner layer. (a) Schematic illustration of PI-HAP/C20 inner layer with thermal management. (b) Radial cross-sectional SEM image of PI-HAP/C20 fiber. (c) FT-IR spectra of PI-HAP and PI-HAP/C20 fiber. (d) DSC curves of C20 and PI-HAP/C20 fiber. (e) The phase-change enthalpy of PI-HAP/C20 fabric compared with previously reported phase change fabrics. (f) Digital images of C20 and PI-HAP/C20 at 80 °C for 0 s and 10 s. (g) The temperature-time curves recorded by thermocouple and (h) infrared thermal images of PI-HAP/C20 fabric and aramid fabric during the heating and cooling process.

C═O (1772 cm^{-1}、 1715 cm^{-1}), C–N (1365 cm^{-1}) [39] and P–O (1000 cm^{-1}) [20] bands of PI-HAP aerogel fibers, additional peaks of C–H band at around 2849, 2914, 2956 cm^{-1}, and C–H_3 stretching vibration band at 1470 cm^{-1} [10] appear for PI-HAP/C20 fiber, corresponding to the stretching vibration attributed to C20, indicating the successful incorporation of C20 within the pore of PI-HAP aerogel fibers.

Owing to the high porosity of PI-HAP aerogel fiber, PI-HAP/C20 fabric exhibits high loading (93 wt%) of C20 as calculated from TGA curves (Fig. S7), which is conducive to obtain the phase-changeable fabric with high phase-change enthalpy. DSC results reveal that T_{onset} (onset temperature of melting) and T_m (melting temperature) of PI-HAP/C20 are near to that of pure C20 at around 32.8 °C and 42.0 °C, respectively (Fig. 3d & Table S4), indicating that the endothermic peak stemmed from the melting of C20. The phase change enthalpy of PI-HAP/C20 fabric calculated from DSC curves is as high as 193.2 J g^{-1}, which is much higher than that of the previous reported PCM composite textiles [40–47] (Fig. 3e), indicating its huge thermal storage capability as the thermoregulation layer. In addition, the DSC curves of PI-HAP/C20 fabric after different heating and cooling cycles is given in Fig. S8, which shows that the T_{onset} and T_m of the curves after different cycles are stable at 32.8 and 42.0 °C, respectively. Moreover, the PI-HAP/C20 fabric presents excellent stability with 93.3% retention of melting enthalpy after 100 heating-cooling cycles (Fig. S9). Besides, due to the strong capillary force of aerogel fiber, no leakage of C20 is

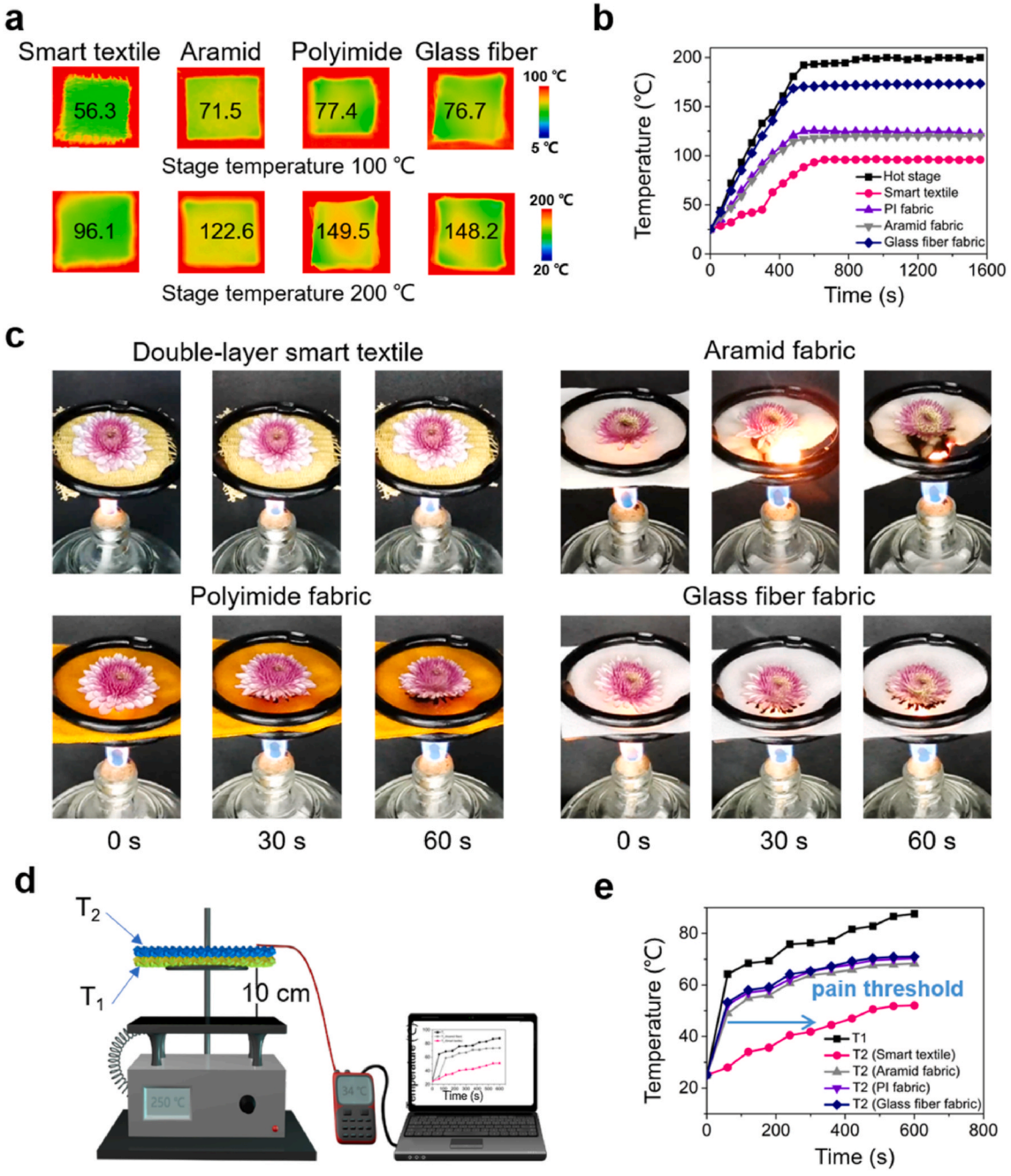

Fig. 4. Firefighting and thermal-protective performance of the double-layer smart textile. (a) Infrared thermal images and (b) corresponding surface temperature versus time curves of smart textile, commercial aramid fabric, polyimide fabric and glass fiber fabric on a hot stage of 100 °C and 200 °C. (c) Optical images of flowers on our smart textile and commercial textiles burning by an alcohol lamp at different times. (d) Schematic illustration of thermal protection test. (e) Temperature change with time of smart textile and commercial fabrics exposed on a hot stage of 250 °C with a distance of 10 cm.

detected when heated to 80 °C (Fig. 3f), reflecting the great potential for prolonged thermal management and utilization in real working occasions.

To evaluate the thermoregulation capability of PI-HAP/C20 fabric under actual conditions, the surface temperature of the phase-changeable fabric was recorded by thermocouple and infrared thermal camera by placing it on the temperature-adjustable stage. The stage was heated from 25 °C to 80 °C and cooled from 80 °C to 25 °C, respectively, which was illustrated in Fig. S10. The related surface temperature changes of the fabrics on the hot stage were recorded by thermocouples, and the temperature-time curves are given in Fig. 3g. Different from commercial aramid fabric, the curve of PI-HAP/C20 fabric exhibits the obvious platforms around 38.5–40.2 °C during heating and cooling, indicating that it can postpone the temperature change during ambient temperature fluctuations. Moreover, according to the corresponding infrared thermal images (Fig. 3h), the surface temperature of PI-HAP/C20 fabric is only 41.7 °C at the end of melting phase change process (the time of t_2), obviously lower than that of commercial aramid fabric (51.5 °C), exhibiting superior cooling ability under hot enviroment. In the process of cooling, PI-HAP/C20 fabric presents higher surface temperature than that of commercial aramid fabric at the end of solidifying phase change process (the time of t_4), with 7.4 °C higher than that of commercial aramid fabric, reflecting its excellent warming performance in the cold environment. Therefore, PI-HAP/C20 fabric exhibits huge thermoregulation capability for enhancing the thermal-protective performance of the double-layer smart textile.

3.3. Firefighting and thermal-protective performance of the double-layer smart textile

The double-layer smart textile was obtained by integrating the PI-HAP-rGO aerogel fabric and PI-HAP/C20 fabric, and the comprehensive performance such as firefighting and thermal-protective property were evaluated. The thermal-protective property of the double-layer textile was compared with other commercial fabric such as aramid fabric, PI fabric and glass fiber fabric with the same thickness of ~2.0 mm. They were placed on the hot stage of 100 °C and 200 °C, respectively, and their corresponding surface temperature was recorded through an infrared thermal camera (Fig. 4a) and thermocouple (Fig. 4b). The related infrared thermal images show that the surface temperature of our smart textile is obvious lower than that of commercial fabrics, presenting much better thermal-protective performance of our smart textile. The equilibrium surface temperature of our smart textile only reaches 96.1 °C on the stage of 200 °C, which is ~26 °C lower than commercial aramid fabric and ~50 °C lower than polyimide fabric and glass fiber fabric, corresponding to excellent thermal insulation performance. The corresponding temperature versus time curves in Fig. 4b also indicate the lowest surface temperature of our smart textile that consistent with the results of infrared thermal images, which gives more evidence for proving its outstanding thermal-protective performance.

The firefighting and thermal-protective properties were further assessed by using the double-layer textile as protective for flowers on fire (Fig. 4c). Specifically, the flower is placed on the top surface of the smart textile that is ignited by an alcohol lamp. It is noted that the flower could keep stable on the top of our smart textile within 60 s while those on the top of commercial fabrics are withered or burned, which is also evident in **Videos S4–S7**. The phenomenon demonstrates the superior firefighting performance of our double-layer textile with both flame-retardant and thermal-protective function, having a huge potential as a new firefighting protective garment.

Supplementary video related to this article can be found at https://doi.org/10.1016/j.compositesb.2022.110377

Furthermore, the double-layer smart textile was exposed on a heat source of 250 °C with a distance of 10 cm, simulating the ambient temperature at the rescue scene, and the temperature change for the outer side (T_1) and inner side (T_2) of smart textile were recorded by thermocouples (Fig. 4d). The lower temperature at the inner side, the cooler skin temperature will be gotten. Normally, it is reported that 44 °C is of the pain threshold for human skin. Fig. 4e gives the related temperature-time curves at the environment and skin side respectively. It is observed obviously that the equilibrium temperature at the outer side (environment) reach around 87.6 °C. As for the temperature at the inner side, commercial fabrics have the approximative equilibrium temperature of around 68.3–71.0 °C, which is just a bit lower than that of outer side. Much different from commercial fabrics, the equilibrium temperature of our smart textile reached to only 52.1 °C, corresponding to excellent thermal-protective property. Moreover, the time to pain threshold of our smart textile is 280.0 s, much longer than that of the commercial aramid fabric (101.0 s) and glass fiber fabric (56.5 s), providing the thermal safety for firefighters. The excellent thermal protective performance of the smart textile is illustrated in Fig. S11 and can be explained as follows. The outer layer of our smart textile has excellent fire and thermal resistance, endowing its shape stability under the high-temperature environment. The excellent thermal regulation property of the inner layer could inhibit the temperature rise of inner side due to the excellent thermal storage ability of phase change fabric, reducing the risk of the skin burn for firefighters. When the outside of our smart textile is heated, a large portion of heat is blocked by PI-HAP-rGO aerogel fabric and other portion is absorbed by C20 of PI-HAP/C20 fabric with high phase-change enthalpy, leading to few heat transferred to the inner side of the double-layer smart textile. Therefore, the flame-retardant outer layer and thermoregulating inner layer can synergistically endow the double-layer smart textile with excellent thermal-protective function as the next generation firefighting protective clothing.

4. Conclusion

In summary, a double-layer textile comprising of flame-retardant PI-HAP-rGO aerogel fabric as outer layer and phase-changeable PI-HAP/C20 fabric as inner layer has been developed, which exhibits outstanding fire-resistant and thermal-protective performance for potential firefighting clothing. Benefiting from the incorporation of the flame-retardant materials of HAP and rGO, PI-HAP-rGO aerogel fabric as outer layer exhibits excellent fire resistance with high LOI value of 47.5% and 70.0% reduction of PHRR compared with commercial aramid fabric. Meanwhile, phase-changeable PI-HAP/C20 fabric as the inner layer has high loading (93 wt%) of C20, endowing high melting enthalpy of 193.2 J g^{-1}, which contributes to strong thermoregulation capability to postpone the temperature rising in the hot environment. Ultimately, the double-layer smart textile offers superior thermal protective effect in terms of delaying around 280.0 s to pain threshold, respectively, much longer than that of the commercial aramid fabric (101.0 s) and glass fiber fabric (56.5 s), which shows great potential as alternative to the next-generation firefighting protective garment.

Credit author statement

Qiaoran Zhang: Investigation, Methodology, Writing - original draft; **Lei Ma**: Investigation, Methodology; **Tiantian Xue** : Investigation, Methodology; **Jing Tian:** Software, Validation; **Wei Fan:** Conceptualization, Supervision, Writing - review & editing; **Tianxi Liu:** Writing - review & editing.

Declaration of competing interest

The authors declare that they have no known competing financial interests or personal relationships that could have appeared to influence the work reported in this paper.

Data availability

Data will be made available on request.

Acknowledgements

This work was supported by the National Natural Science Foundation of China (52073053), Young Elite Scientists Sponsorship Program by CAST (2021QNRC001), Shanghai Rising-Star Program (21QA1400300), Innovation Program of Shanghai Municipal Education Commission (2021-01-07-00-03-E00108), Science and Technology Commission of Shanghai Municipality (20520741100), and China Postdoctoral Science Foundation (2021M690596).

Appendix A. Supplementary data

Supplementary data to this article can be found online at https://doi.org/10.1016/j.compositesb.2022.110377.

References

[1] Naeem J, Mazari A, Volesky L, Mazari F. Effect of nano silver coating on thermal protective performance of firefighter protective clothing. J Textil Inst 2018;110(6):847–58.
[2] Chou C, Tochihara Y, Kim T. Physiological and subjective responses to cooling devices on firefighting protective clothing. Eur J Appl Physiol 2008;104(2):369–74.
[3] Hu Y, Huang D, Qi Z, He S, Yang H, Zhang H. Modeling thermal insulation of firefighting protective clothing embedded with phase change material. Heat Mass Tran 2012;49(4):567–73.
[4] Easson MW, Jordan JH, Chang S, Bland JM, Condon BD. Investigation of bisphenol-substituted spirocyclic phosphazenes as cotton textile–based flame retardants. J Eng Fiber Fabr 2020;15:1–10.
[5] Yang W, Wang NN, Ping P, Yuen AC, Li A, Zhu SE, et al. Novel 3D network architectured hybrid aerogel comprising epoxy, graphene, and hydroxylated boron nitride nanosheets. ACS Appl Mater Interfaces 2018;10(46):40032–43.
[6] Fan W, Zhang X, Zhang Y, Zhang Y, Liu T. Lightweight, strong, and super-thermal insulating polyimide composite aerogels under high temperature. Compos Sci Technol 2019;173:47–52.
[7] Li M, Chen X, Li X, Dong J, Zhao X, Zhang Q. Controllable strong and ultralight aramid nanofiber-based aerogel fibers for thermal insulation applications. Adv Fiber Mater 2022. https://doi.org/10.1007/s42765-022-00175-2.
[8] Qi ZK, Huang DM, He S, Yang H, Hu Y, Li LM, Zhang HP. Thermal protective performance of aerogel embedded firefighter's protective clothing. J Eng Fibers Fabr 2013;8(2):134–8.
[9] Shaid A, Wang L, Padhye R. The thermal protection and comfort properties of aerogel and PCM-coated fabric for firefighter garment. J Ind Textil 2015;45(4):611–25.
[10] Shaid A, Furgusson M, Wang L. Thermophysiological comfort analysis of aerogel nanoparticle incorporated fabric for fire fighter's protective clothing. Chem Mater Engineer 2014;2(2):37–43.
[11] Wang YJ, Cui Y, Shao ZY, Gao WW, Fan W, Liu TX, et al. Multifunctional polyimide aerogel textile inspired by polar bear hair for ther-moregulation in extreme environments. Chem Eng J 2020;390:124623.
[12] Li X, Dong G, Liu Z, Zhang X. Polyimide aerogel fibers with superior flame resistance, strength, hydrophobicity, and flexibility made via a universal sol-gel confined transition strategy. ACS Nano 2021;15(3):4759–68.
[13] Serbezeanu D, Popa AM, Stelzig T, Sava I, Rossi RM, Fortunato G. Preparation and characterization of thermally stable polyimide membranes by electrospinning for protective clothing applications. Textil Res J 2015;85(17):1763–75.
[14] Shang Z, Lü C, Lü X, Gao L. Synthesis and properties of silica–polyimide hybrid films derived from colloidal silica particles and polyamic acid. J Appl Polym Sci 2008;109(6):3477–83.
[15] Li Y, Fu SY, Li YQ, Pan QY, Xu G, Yue CY. Improvements in transmittance, mechanical properties and thermal stability of silica–polyimide composite films by a novel sol–gel route. Compos Sci Technol 2007;67(11–12):2408–16.
[16] Cao J, Wang Z, Yang X, Tu J, Wu R, Wang W. Green synthesis of amphipathic graphene aerogel constructed by using the framework of polymer-surfactant complex for water remediation. Appl Surf Sci 2018;444:399–406.
[17] Hou Y, Qiu S, Hu Y, Kundu CK, Gui Z, Hu W. Construction of bimetallic ZIF-derived Co-Ni LDHs on the surfaces of GO or CNTs with a recyclable method: toward reduced toxicity of gaseous thermal decomposition products of unsaturated polyester resin. ACS Appl Mater Interfaces 2018;10(21):18359–71.
[18] Yu Y, Pan D, Zhao L, Huang S, Lin P, Wang Z, et al. Paper-like polyphenylene sulfide/aramid fiber electrode with excellent areal capacitance and flame-retardant performance. Adv Fiber Mater 2022. https://doi.org/10.1007/s42765-022-00176-1.
[19] Wang YT, Zhao HB, Degracia K, Han LX, Sun H, Sun M, et al. Green approach to improving the strength and flame retardancy of poly(vinyl alcohol)/clay aerogels: incorporating biobased gelatin. ACS Appl Mater Interfaces 2017;9(48):42258–65.
[20] Guo WW, Liu JJ, Zhang P, Song L, Wang X, Hu Y. Multi-functional hydroxyapatite/polyvinyl alcohol composite aerogels with self-cleaning, superior fire resistance and low thermal conductivity. Compos Sci Technol 2018;158:128–36.
[21] Peng H, Wang D, Zhang L, Li M, Liu M, Wang C, et al. Amorphous cobalt borate nanosheets grown on MoS_2 nanosheet for simultaneously improving the flame retardancy and mechanical properties of polyacrylonitrile composite fiber. Compos B Eng 2020;201:108298.
[22] Wang D, Peng H, Yu B, Zhou K, Pan H, Zhang L, et al. Biomimetic structural cellulose nanofiber aerogels with exceptional mechanical, flame-retardant and thermal-insulating properties. Chem Eng J 2020;389:124449.
[23] Lu Y, Xiao XD, Fu J, Huan CM, Shuai S, Zhan YJ, et al. Novel smart textile with phase change materials encapsulated core-sheath structure fabricated by coaxial electrospinning. Chem Eng J 2019;355:532–9.
[24] Yu X, Li Y, Yin X, Wang XF, Han YH, Si Y, et al. Corncoblike, superhydrophobic, and phase-changeable nanofibers for intelligent thermoregulating and water-repellent fabrics. ACS Appl Mater Interfaces 2019;11(42):39324–33.
[25] Wu Y, Chen CC, Jia YF, Wu J, Huang Y, Wang LG. Review on electrospun ultrafine phase change fibers (PCFs) for thermal energy storage. Appl Energy 2018;210:167–81.
[26] Xia W, Xiang H, Zhou Z, Fei X, Zhu M. Hybridizing rational designed hydrophobic PEG-based derivatives into nanoporous F–SiO_2 as form-stable phase change materials for melt-spun PA6 phase change fibers with a superior washing durability. Compos Commun 2021;24:100633.
[27] Huang J, Yu H, Abdalkarim SYH, Marek J, Militky J, Li Y, et al. Electrospun polyethylene glycol/polyvinyl alcohol composite nanofibrous membranes as shape-stabilized solid–solid phase change materials. Adv Fiber Mater 2020;2(3):167–77.
[28] Meng Y, Majoinen J, Zhao B, Rojas OJ. Form-stable phase change materials from mesoporous balsa after selective removal of lignin. Compos B Eng 2020:199.
[29] Xiao YY, He YJ, Wang RQ, Lei YZ, Yang JH, Qi XD, et al. Mussel-inspired strategy to construct 3D silver nanoparticle network in flexible phase change composites with excellent thermal energy management and electromagnetic interference shielding capabilities. Compos B Eng 2022:239.
[30] Li J, Zhu X, Wang H, Lin P, Jia L, Li L, et al. Synthesis and properties of multifunctional microencapsulated phase change material for intelligent textiles. J Mater Sci 2020;56(3):2176–91.
[31] Li X, Wang C, Wang Y, Wang B, Feng X, Mao Z, et al. Flexible and resilient photothermal polyurethane film from polydopamine-coated phase change microcapsules. Sol Energ Mat and Sol C 2021:227.
[32] Zhao X, Yang F, Wang Z, Ma P, Dong W, Hou H, et al. Mechanically strong and thermally insulating polyimide aerogels by homogeneity reinforcement of electrospun nanofibers. Compos B Eng 2020;182:107624.
[33] Cui Y, Gong H, Wang Y, Li D, Bai H. A thermally insulating textile inspired by polar bear hair. Adv Mater 2018;30(14):1706807.
[34] Yuan S, Fan W, Wang D, Zhang L, Miao YE, Lai F, et al. 3D printed carbon aerogel microlattices for customizable supercapacitors with high areal capacitance. J Mater Chem 2021;9(1):423–32.
[35] Fu Q, Medina L, Li Y, Carosio F, Hajian A, Berglund LA. Nanostructured wood hybrids for fire-retardancy prepared by clay impregnation into the cell wall. ACS Appl Mater Interfaces 2017;9(41):36154–63.
[36] Zhang QR, Li ZW, Li XH, Yu LG, Zhang ZJ, Wu ZS. Zinc ferrite nanoparticle decorated boron nitride nanosheet: preparation, magnetic field arrangement, and flame retardancy. Chem Eng J 2019;356:680–92.
[37] Xu W, Wang X, Wu Y, Li W, Chen C. Functionalized graphene with Co-ZIF adsorbed borate ions as an effective flame retardant and smoke suppression agent for epoxy resin. J Hazard Mater 2019;363:138–51.
[38] Guo W, Wang X, Zhang P, Liu J, Song L, Hu Y. Nano-fibrillated cellulose-hydroxyapatite based composite foams with excellent fire resistance. Carbonhyd Polym 2018;195:71–8.
[39] Guo CY, Wang QW, Liu JG, Qi L, Huangfu MG, Wu X, et al. Electrospun polyimide ultrafine non-woven fabrics with high whiteness and good thermal stability from organo-soluble semi-alicyclic polyimides: preparation and properties. Express Polym Lett 2019;13(8):724–38.
[40] Jesse T. McCann MM, Younan Xia. Melt coaxial electrospinning: a versatile method for the encapsulation of solid materials and fabrication of phase change nanofibers. Nano Lett 2006;6:2868–72.
[41] Sirohi S, Singh D, Nain R, Parida D, Agrawal AK, Jassal M. Electrospun composite nanofibres of PVA loaded with nanoencapsulated n-octadecane. RSC Adv 2015;5(43):34377–82.
[42] Perez-Masia R, Lopez-Rubio A, Fabra MJ, Lagaron JM. Biodegradable polyester-based heat management materials of interest in refrigeration and smart packaging coatings. J Appl Polym Sci 2013;130(5):3251–62.
[43] Zhao L, Luo J, Li Y, Wang H, Song G, Tang G. Emulsion-electrospinning n-octadecane/silk composite fiber as environmental-friendly form-stable phase change materials. J Appl Polym Sci 2017;134(47).
[44] Do CV, Nguyen TTT, Park JS. Phase-change core/shell structured nanofibers based on eicosane/poly(vinylidene fluoride) for thermal storage applications. Kor J Chem Eng 2013;30(7):1403–9.
[45] Ke H, Li D, Zhang H, Wang X, Cai Y, Huang F, et al. Electrospun form-stable phase change composite nanofibers consisting of capric acid-based binary fatty acid eutectics and polyethylene terephthalate. Fibers Polym 2013;14(1):89–99.
[46] Pérez-Masiá R, López-Rubio A, Lagarón JM. Development of zein-based heat-management structures for smart food packaging. Food Hydrocolloids 2013;30(1):182–91.
[47] Zong X, Cai YB, Sun GY, Zhao Y, Huang FL, Song L, Hu Y, Fong H, Wei S, F Q. Fabrication and characterization of electrospun SiO_2 nanofibers absorbed with

fatty acid eutectics for thermal energy storage/retrieval. Sol Energ Mat Sol C 2015; 132:183–90.